Development and evaluation of cancer-targeted pre-operative and intra-operative dual-imaging probes based on metal nanoparticles

（金属ナノ粒子を基盤とするがん標的術前・術中

デュアルイメージングプローブの開発と評価）

Digest（要約）

2019

DING NING

Table of Contents

Abbreviations

The abbreviations used in this dissertation are as follows;

magnetic resonance imaging (MRI)

^{18}F-fluorodeoxyglucose (FDG)

positron emission tomography (PET)

indocyanine green (ICG)

photoacoustic imaging (PAI)

gold nanorods (AuNRs)

iron oxide nanoparticles (IONPs)

surface plasmon resonance (SPR)

enhanced permeability and retention (EPR)

single photon emission computed tomography (SPECT)

human epidermal growth factor receptor 2 (HER2)

1-ethyl-3-(3-dimethylaminopropyl)-carbodiimide (EDC)

N-hydroxysulfosuccinimide sodium salt (Sulfo-NHS)

2-(*N*-morpholino)ethanesulfonic acid (MES)

phosphate buffered saline (PBS)

phosphate buffered saline with Tween20 (PBST)

polyethylene glycol (PEG)

diethylenetriaminepentaacetic acid (DTPA)

sodium dodecyl sulfate (SDS)

ethylenediaminetetraacetic acid (EDTA)

transmission electron microscopy (TEM)

region of interest (ROI)

Introduction

Cancer has long been a main cause of death worldwide[1]. In Japan, cancer has been the leading cause of mortality for >30 years, and mortality rates have trended upward[2].

Among various cancer therapies, surgery remains one of the main treatments for many types of solid tumors with >50% of cancer patients undergoing surgery each year[3]. In fact, the cure rate of most solid tumor types can be increased by 4–11 folds by surgical excision[4]. To remove as much tumor tissue as possible, both highly precise pre-operative and intra-operative imaging diagnosis are necessary[5,6]. Pre-operative diagnostic techniques, such as nuclear medicine [positron emission tomography (PET) and single photon emission computed tomography (SPECT) are the representative ones] and magnetic resonance imaging (MRI), can facilitate identification of tumors. During surgeries, incomplete tumor resection remains a major challenge and occurs as much as 20% to 60% among all operations[3]. Intra-operative diagnoses, which are usually made by performing optical imaging, can identify small tumor lesions, locate metastases, help complete tumor removal, and thus guide surgeons in operating and by enabling real‑time decisions during surgery[7].

Currently, it is common to use different probes for pre-operative and intra-operative diagnosis, such as ^{18}F-fluorodeoxyglucose (FDG) for PET and indocyanine green (ICG) for fluorescence imaging[8-11], however, this might cause information discrepancies and difficulties in localization of tumors during surgery. Thus, the development of probes that could provide identical information in pre- and intra-operative diagnosis is essential for precise cancer therapy. Dual-imaging probes not only provide complementary information for diagnosis, but also bridge the gap between surgical planning and image-guided resection with a single, molecular targeting probe.

In recent years, photoacoustic imaging (PAI) has emerged as a new type of biomedical diagnostic method based on the PA effect, which is the formation of ultrasound waves following light absorption

in optical absorbers. The quantification of the sound formed by the PA effect by using transducers enables obtaining the photoacoustic signal[12]. The reconstruction of PA signals forms PA images. Ultrasound waves exhibit much lower tissue scattering, which leads to penetration depths of multiple centimeters and spatial resolution at the sub-millimeter level. Thus, PAI has the potential for a broader clinical and intra-operative application than offered by other forms of optical imaging, and development of PAI probes for tumor imaging has been strongly desired[13].

A PAI probe requires both strong absorption in the near-infrared region of the optical spectrum for high permeability through the body and generation of a strong PA response. Although there are other materials such as fluorescence dyes that can be used as PAI probes, in this study, the author chose to use metal nanoparticles [gold nanorods (AuNRs) and iron oxide nanoparticles (IONPs)] for the following reasons. First, these nanoparticles have strong and tunable optical absorptions because of the surface plasmon resonance (SPR) effect[14]. Second, the size of nanoparticles gives an advantage of much greater accumulation of the nanoparticles in tumor tissue than in normal tissues, which is known as the enhanced permeability and retention (EPR) effect[15]. Finally, many attempts have been made to modify the surfaces of metal nanoparticles, to make it possible to further optimize the accumulation and affinity toward tumor, and to easily modify the particles for applications in other pre-operative diagnostic imaging techniques for pre-operative diagnoses such as SPECT. Furthermore, IONPs themselves can be clinically utilized as an MRI probe[16].

Finally, human epidermal growth factor receptor 2 (HER2) was chosen as the target molecule for diagnosis of tumors for the following reasons: it has a close association with a poor prognosis[17]; it is highly expressed in various cancers including breast, ovarian, and gastric cancer, some of which have the highest mortality rates[18]; and HER2 is one of the most thoroughly-researched cancer-related biomarkers, which makes differential diagnosis even more necessary.

Therefore, the study aim was to develop and evaluate of HER2 positive cancer-targeted pre-

operative and intra-operative dual-imaging probes based on metal nanoparticles.

Chapter Descriptions

Chapter 1 presents the preparation and investigation of the feasibility of using radiolabeled anti-HER2 monoclonal antibody (trastuzumab)-conjugated AuNRs as PAI and SPECT probes.

Chapter 2 presents the preparation and investigation of the feasibility of using anti-HER2 scFv-IONPs as PAI and MRI probes.

Chapter 3 presents the preparation and investigation of the feasibility of using trastuzumab-conjugated liposome encapsulated with IONPs as PA and MR dual-imaging probes.

Chapter 1

Preparation and investigation of the feasibility of using radiolabeled anti-HER2 monoclonal antibody (trastuzumab)-conjugated AuNRs as PAI and SPECT probes (digest)

AuNRs were chosen as the photosensitizers. AuNRs possess an excellent photothermal conversion ability because they have strong and tunable localized surface plasmon resonance (SPR) effect[19-21]. This photothermal conversion ability ensures that AuNRs can efficiently generate PA signals, and thereby enable the use of AuNRs as an intra-operative PAI probe.

In this section, to target HER2, anti-HER2 monoclonal antibody (trastuzumab) was chosen as the ligand and conjugated to the surface of AuNRs and the compound is referred to as trastuzumab-AuNRs or Tra-AuNRs for short. To achieve pre-operative HER2 imaging, the author focused on SPECT. SPECT is a nuclear medical imaging technique widely used in clinics that enables whole-body scanning. Indium-111 (^{111}In; $t_{1/2}$ = 2.8 days; γ-radiation, 171 keV, 254 keV) is one of the commonly used radioisotopes that are applicable to SPECT imaging, and trastuzumab in Tra-AuNRs can be efficiently radiolabeled with ^{111}In by using diethylene triamine pentaacetic acid (DTPA) as a metal chelator.

In this chapter, by adjusting the reaction conditions, the author prepared a ^{111}In-labeled Tra-AuNRs (^{111}In-Tra-AuNRs) series with different amounts of trastuzumab conjugated with AuNR. The binding affinities of the Tra-AuNRs series toward HER2 positive N87 cells were evaluated, followed by investigation of the biodistribution in HER2-positive and HER2-negative (SUIT2) tumor-bearing mice. The one represented better binding affinity to HER2 as well as HER2-selective tumor accumulation *in vivo* was considered to be suitable for further imaging studies. Finally, the author conducted an *in vivo* SPECT imaging study using the chosen ^{111}In-Tra-AuNRs. The HER2-specific *in*

vivo tumor imaging was achieved 96 h after probe administration, which suggested that this probe has a potential as a PA/SPECT dual imaging probe targeting HER2-positive tumors.

Chapter 2

Preparation and investigation of the feasibility of using anti-HER2 scFv-IONPs as PAI and MRI probes

Although Tra2-AuNRs demonstrated partial HER2-specific tumor accumulation *in vivo*, it was difficult to perform earlier post-injection imaging due to the slow clearance from the blood. It is reported that rod-like nanoparticles possess a longer lifetime in the blood stream than sphere-like particles[22]. AuNRs have an absorbance peak in the near-infrared (NIR) window (650–1350 nm) in which the absorbance by water and hemoglobin is at minimum[23]. However, sphere gold nanoparticles have absorbance peaks in the range of 500–600 nm[24], which is not suitable for *in vivo* imaging. In order to overcome this problem, the author considered that IONPs, sphere-like nanoparticles approved clinically, seemed promising as a platform for PA/MR dual imaging due to the following reasons. In this research, the feasibility of using scFv-IONPs as PA/MR dual-imaging probes was investigated.

IONPs were first approved by the United States Food and Drug Administration (FDA) in 1996 (GastroMARK®) as an oral negative MR contrast agent[25] to distinguish the loops of bowel from other abdominal structures and physiology. Then onwards, other intravenous IONPs have been approved in the 2000s (such as Resovist® approved in 2001 for the European market), and have been used successfully in some instances of liver tumor enhancement due to the nonspecific uptake of the IONPs by the mononuclear phagocyte system or reticuloendothelial system (RES) after intravenous administering[26,27]. Advances in nanotechnology resulted in further systematic development of IONPs including variation in particle size and coating modification[28], and in recent years there has been renewed interests in IONPs as multifunctional vehicles[28,29]. Meanwhile, many attempts have been devoted on labeling IONPs with targeting moieties such as antibody to achieve non-invasive detection of overexpressed tumor surface antigens by MRI[28,30]. Furthermore, it is reported that IONPs, being

able to improve the sensitivity and spectroscopic specificity of a PA signal, can enhance the performance of a PA system[31]. Thus, utilizing of IONPs can lead to discrimination of tumor malignancy and determination of suitable therapeutic strategy. In fact, we previously reported that IONPs conjugated with anti-HER2 single-chain Fv (scFv) demonstrated potential as an HER2-targeted PAI probe, and a study using IONPs approved clinically as a platform for PA/MR dual imaging was conducted. In this research, the feasibility of using scFv-IONPs as PA/MR dual-imaging probes was investigated.

2-1 Results and discussion

2-1-1 Characterization of IONPs and scFv-IONPs

The scFv-IONPs were prepared by conjugation of anti-HER2 scFv to maleimide groups on the surface of nanomag®-CLD-spio. The particle size of IONPs and scFv-IONPs was 40.0 ± 8.6 and 47.5 ± 10.8 nm, respectively. Compared with unmodified IONP, the size of scFv-IONPs increased due to conjugation of the 9.7 ± 1.7 scFv molecules per IONP conjugation while the zeta potential hardly changed. The zeta potentials of IONPs and scFv-IONPs were 3.7 ± 1.5 and 3.2 ± 1.3 mV, respectively.

The transverse relaxivity (*r2*) of IONPs and scFv-IONPs was 261.6 ± 14.7, and 296.3 ± 43.3 $mM^{-1}s^{-1}$, respectively, determined by MRI machine (MRmini SA), showing no significant change due to scFv conjugation. The signal of the 0.2 mM iron concentration phantom was too low, therefore, *R2* at 0.2 mM could not be precisely measured (Figure 2-1).

The dissociation constant to HER2 (K_d) for the interaction between scFv-IONPs and HER2 was determined 11.7 ± 7.3 nM by cellular binding assay.

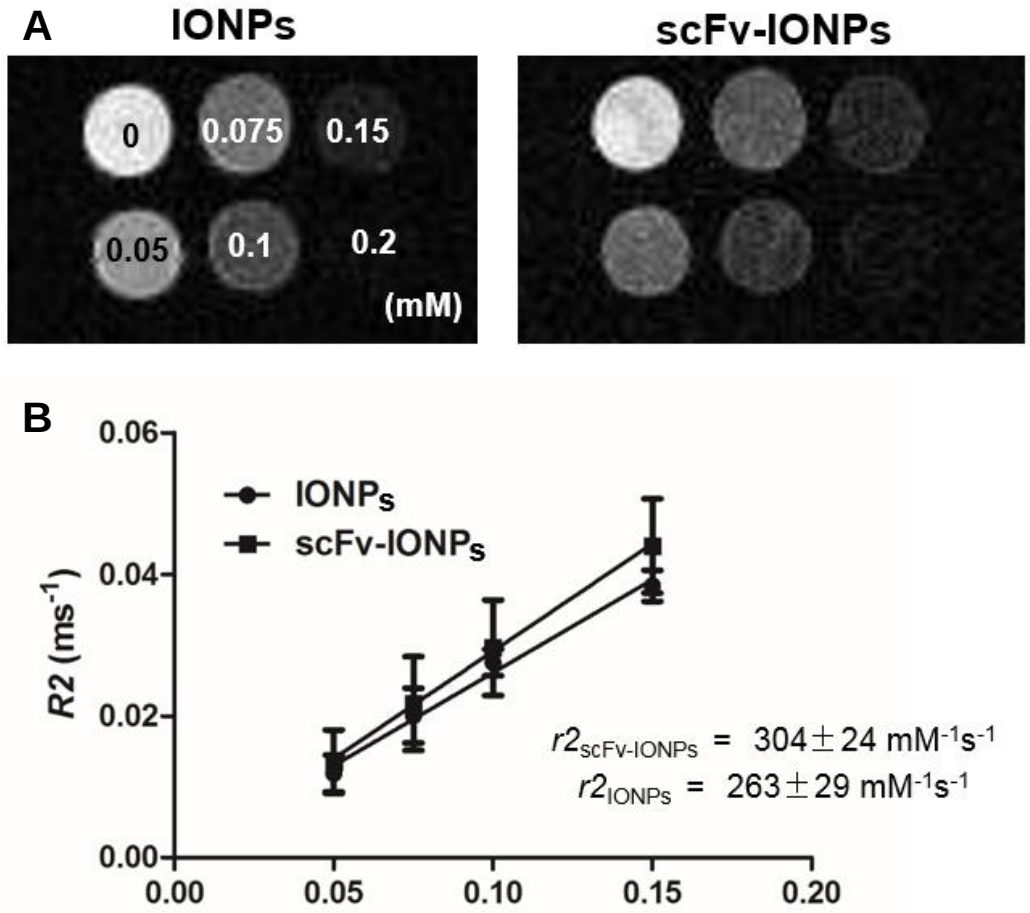

Figure 2-1. Measurement of transverse relaxivity (*r2*).

A. Representative MR images of IONPs and scFv-IONPs phantom solutions with different iron concentrations.

B. Relationship between the transverse relaxation rate (*R2*) and the iron concentration. The slope of the regression line corresponds to the transverse relaxivity (*r2*). The *r*2 values for IONPs and scFv-IONPs were 261.6 and 296.3 $mM^{-1}s^{-1}$, respectively (mean ± SD, n = 3).

2-1-2 *In vitro* MRI studies

The specific binding to HER2-overexpressing N87 cells of scFv-IONPs was further proved by *in vitro* MR studies. As described in Figure 2-2, N87 cells labeled by scFv-IONPs displayed negative contrast enhancement in *T2*-weighted MR images, in which the signal significantly decreased by 44.6 ± 7.8% than that in the control cells. This decrease in MR signal was inhibited by co-incubation of excess trastuzumab. Moreover, the MR signal of PEG-IONPs (without scFv) in N87 cells did not change. Furthermore, the MR signal intensity was not altered by the treatment of SUIT2 cells (HER2

low expression) with scFv-IONPs. These results demonstrated the HER2-specific binding of scFv-IONPs *in vitro*.

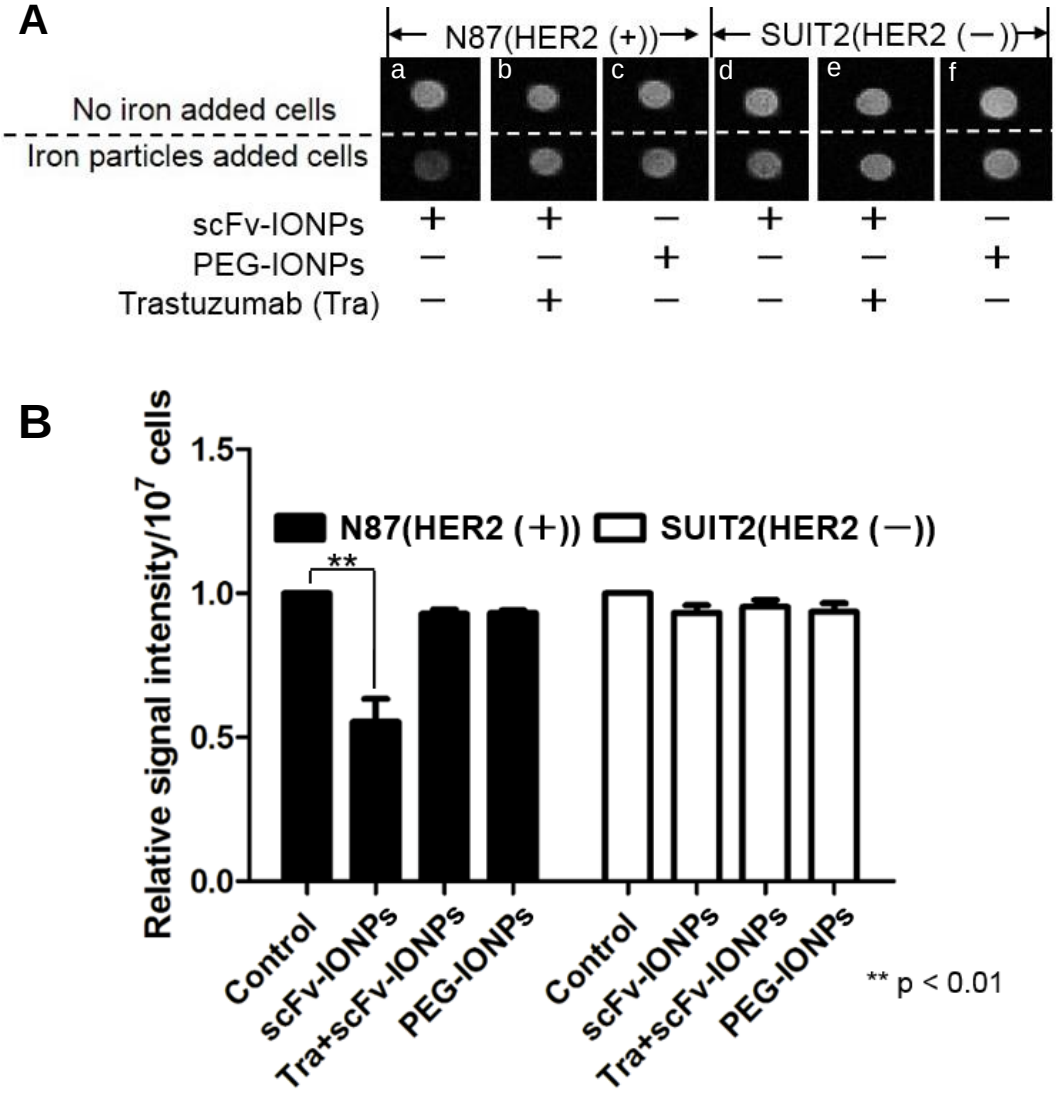

Figure 2-2. *In vitro* cellular binding assay of the IONPs conjugated with or without anti-HER2 scFv.
A. Representative MR images of the cells collected in tubes. a. scFv-IONP in N87; b. scFv-IONP (trastuzumab pre-treated) in N87; c. PEG-IONP in N87; d. scFv-IONP in SUIT2; e. scFv-IONP (trastuzumab pre-treated) in SUIT2; f. PEG-IONP in SUIT2.
B. The relative MR signal intensity per 10^7 cells calculated from *in vitro* MR images (mean ± SD, n = 3) . ** $p < 0.01$ vs Control.

2-1-3 *In vivo* MRI studies

MR images were acquired with scFv-IONPs or PEG-IONPs in the N87 and SUIT2 tumor-bearing mice. At 24 h after injection of scFv-IONPs, MR signals in the N87 tumors significantly decreased than that in the SUIT2 (Figure 2-3A). Meanwhile, less decrease in the signal of PEG-IONPs was observed in both N87 and SUIT2 tumors. The percentage of signal decrease was 19.3 ± 5.3%, 8.4 ± 2.6%, 6.2 ± 2.5%, and 5.1 ± 1.3%, for scFv-IONPs in N87 tumor, PEG-IONPs in N87 tumor, scFv-IONPs in SUIT2 tumor, and PEG-IONPs in SUIT2 tumor, respectively (Figure 2-3B). As for the *in vivo* blocking study, the accumulation of scFv-IONPs in N87 tumors was inhibited by co-injection of excess trastuzumab and the signal decrease was 10.2 ± 3.7% and 4.2 ± 2.7% for N87 and SUIT2 tumor, respectively. The scFv-IONPs statistically demonstrated HER2-specific tumor uptake and the decrease in MR signals *in vivo* as well as *in vitro*.

Meanwhile, although the MR signal changes of scFv-IONPs- and PEG-IONPs-injected N87 tumors were significantly different ($p < 0.01$), the decrease of MR signals could be also seen in PEG-IONPs-administered N87 tumors as well (Figure 2-3B). This is partially due to non-specific tumor uptake *via* EPR effect and by tumor-associated macrophages presenting in most tumors[32,33]. It suggested that the limitations of this current probe and further modification to enhance tumor accumulation as well as lower particle opsonization[9] would be required in order to be employed in MR diagnosis.

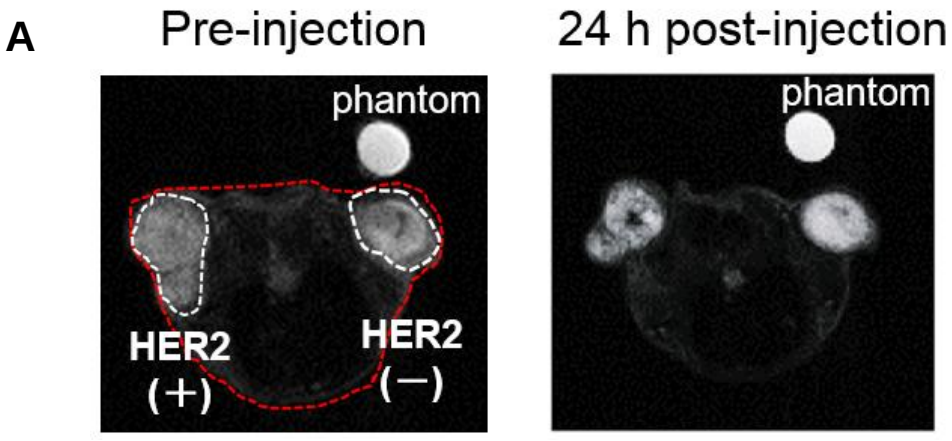

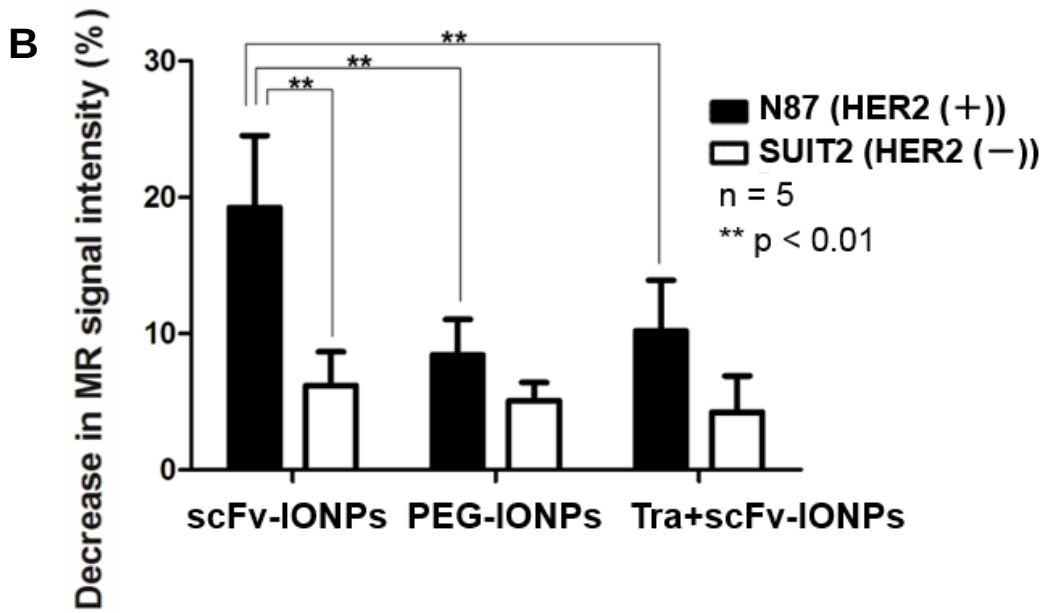

Figure 2-3. *In vivo* MR tumor imaging with scFv-IONPs or PEG-IONPs in N87 and SUIT2 tumor-bearing mice.

A. *In vivo* MR images (transverse plane) of scFv-IONP in N87 (HER2 (+)) and SUIT2 (HER2 (-)) tumor bearing mice. The red line showed the outline of mouse's body in transverse plane, and the white circles indicated transplanted tumors.

B. Decrease in MR signal intensity calculated from *in vivo* MR images using the following equation: Decrease in MRI signal (%) = $[1-({}_{post}ROI_{tumor}/{}_{post}ROI_{phantom})/({}_{pre}ROI_{tumor}/{}_{pre}ROI_{phantom})]\times100$ (mean ± SD, n = 5). **p < 0.01.

2-1-4 IONPs staining

In order to evaluate the uptake of IONPs in the tumor, iron staining of tumor sections was carried out. The slices of N87 and SUIT2 tumors excised from the mice injected with scFv-IONPs or PEG-IONPs were stained using Berlin blue staining set (Figure 2-4). The blue spots derived from IONPs were notable in N87 tumor that was injected with scFv-IONPs and the accumulation was obviously higher than that in the SUIT2 tumor (Figure 2-4A and B). Meanwhile, low amount of IONPs was observed in both N87 and SUIT2 tumor injected with PEG-IONPs (Figure 2-4C and D), which was consistent with the *in vivo* MR studies and our previous report.

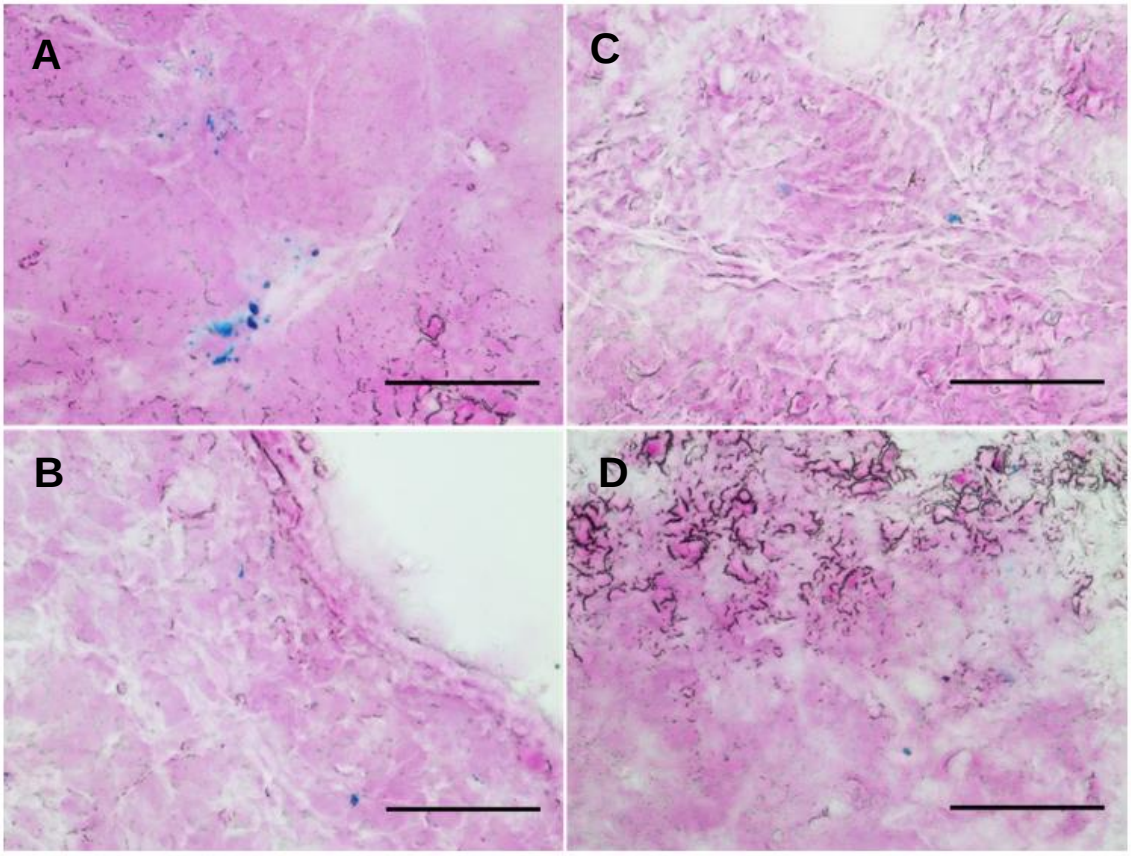

Figure 2-4. *Ex vivo* IONP distribution in the tumor.
The tumors were excised from N87 and SUIT2 tumor-bearing mice injected with scFv-IONPs or PEG-IONPs. Iron staining using Berlin blue and nucleus staining using Nuclear fast red was performed. Scale bar = 100 μm.
A. N87 tumor excised from mice injected with scFv-IONPs.
B. SUIT2 tumor excised from mice injected with scFv-IONPs.
C. N87 tumor excised from mice injected with PEG-IONPs.
D. SUIT2 tumor excised from mice injected with PEG-IONPs.

2-2 Summary

In this chapter, the author designed, synthesized and evaluated anti-HER2 single chain Fv-conjugated iron oxide nanoparticles (scFv-IONPs) as MRI probes. In phantom study, scFv-IONPs showed high transverse relaxivity. In binding affinity study, high affinity to HER2 positive cells was confirmed. The scFv-IONPs also significantly decreased both *in vitro* and *in vivo* MR signals in the

HER2 positive N87 cells and N87 tumors. Together with the conclusion from our previous studies on the scFv-IONPs' potential as a PAI agent, these results suggest that scFv-IONPs would serve as a robust cancer-targeted PA/MR dual imaging probe.

2-3 Experimental

2-3-1 Synthesis of anti-HER2 scFv-conjugated iron oxide nanoparticles (scFv-IONPs)

ScFv-IONPs were prepared according to our previous report[34] by using nanomag®-CLD-spio (diameter 20 nm, Corefront Co. (Tokyo, Japan)) instead of nanomag®-D-spio (diameter 20 nm, Corefront Co., Tokyo, Japan)). In order to conjugate anti-HER2 scFv to iron oxide nanoparticles by forming thioether bond with maleimide groups on the particle surface, anti-HER2 scFv was reduced using tris(2-carboxyethyl)phosphine (Thermo Fisher Scientific Inc., Waltham, MA, USA) for 2 h followed by mixing with iron oxide nanoparticles nanomag®-CLD-spio and incubation at r.t. for 4 h. After anti-HER2 scFv was conjugated to nanomag®-CLD-spio, thiol PEG (MW = 1000, Nanocs. Inc., New York, NY, USA) was added to the mixture to quench the maleimide groups of the particles followed by 1 h of incubation at r.t. and overnight incubation at 4°C. The mixture was electrophoresed to determine the amount of unreacted scFv. The number of anti-HER2 scFv bound to IONPs was quantified by subtracting unconjugated anti-HER2 scFv from the total amount of scFv added. To remove the unreacted scFv, the mixture was purified by dialyzing against PBS with Float-A-Lyzer® G2 (Spectra/Por®, MWCO 300 kDa, SpectrumLabs Com., Rancho Dominguez, CA, USA).

On the other hand, as a control probe, IONPs conjugated with PEG (PEG-IONPs) were prepared by reacting nanomag®-CLD-spio with thiol PEG followed by incubation at r.t. for 1 h and incubation at 4°C overnight and was purified in the same way as scFv-IONPs.

2-3-2 Physicochemical properties of scFv-IONPs

The particle size and zeta potential were measured by Zetasizer Nano ZS (Malvern Instruments, Ltd., Worcestershire, UK) both at 25°C in PBS. The concentration of iron in the particles was measured as previously described[35].

2-3-3 Calculation of *r2*

To measure the transverse relaxivity (*r2*) of scFv-IONPs, phantom studies were performed using a MR system designed for small animals (MRmini SA (1.5 T), DS Pharma Biomedical, Osaka, Japan). Nanomag®-CLD-spio and scFv-IONPs were diluted in PBS with iron concentrations ranging from 0 to 0.2 mM. The solutions were put into the φ38.5 mm RF coil and imaged using a 2-dimentional multi-slice *T2*-weighted sequence (2D-MS, *T2*W). The parameters are as follows. Average = 4; pulse repetition time (TR) = 2000 ms; echo time (TE) = 70, 100, 150, and 200 ms; slice thickness = 1 mm; slice number = 15; field of view = 30×60 mm^2; matrix size = 256×128; flip angle = 90°. Using ImageJ software, the region of interest (ROI) of each solution was drawn and the signal intensity was measured. *R2* was obtained by fitting the logarithm of MR signal intensity vs TE, and *r2* was obtained from the slope of the regression line between *R2* and concentrations of IONPs or scFv-IONPs.

2-3-4 Cell culture

Cell culture of N87 and SUIT2 cells were performed according to the method in Chapter 1.

2-3-5 Binding affinity of scFv-IONPs to HER2

The binding affinity of scFv-IONPs to HER2 was evaluated by calculating the K_d values. HER2-expressing N87 cells were seeded in 24-well plate (4×10^5 cells/well) and incubated in a 5% CO_2/air incubator at 37°C for 16 h. The scFv-IONPs were dissolved in FBS-free DMEM and added to cells

followed by incubation for 1 h at 4°C. As a blocking group, the mixture of scFv-IONPs and excess trastuzumab was added to cells. The iron concentration of scFv-IONPs ranged from 1 to 200 μg/mL, while the concentration of trastuzumab ranged from 4 to 800 μg/mL (n_{scFv}: $n_{trastuzumab}$ = 1:100). After incubation, DMEM was removed and cells were washed twice by PBS at 4°C. Triton X (1%) and HCl (12 M) was added as 100 μL/well to lyse the cells and to denature the iron particles. The binding of scFv-IONPs to HER2 was confirmed by measuring the amount of iron, which was determined based on the absorbance at 535 nm as mentioned previously.

2-3-6 *In vitro* MRI studies

N87 or SUIT-2 cells were cultured in 75 cm^2 flask (1×10^7 cells) for 16 h, followed by removal of the medium and washing twice with PBS. The scFv-IONPs or PEG-IONPs in FBS-free DMEM medium was added to the flask (m_{iron} = 0.5 μg). For blocking studies, N87 and SUIT2 cells were pre-incubated with trastuzumab in FBS-free DMEM medium ($m_{trastuzumab}$ = 20 μg, n_{scFv}:$n_{trastuzumab}$ = 1:1000) for 1 h before the addition of scFv-IONPs to the flasks. After 4 h incubation at 37°C, 1×10^7 cells were collected in tubes, and additionally washed twice with PBS. N87 or SUIT2 cells without added IONPs were collected as control. The centrifuged cells were put into φ38.5 mm RF coil of MRmini SA, and images were taken under the following condition: 2D-MS, *T2*W, Average = 4; TR = 2000 ms; TE = 70 ms; slice thickness = 1 mm; slice number = 33. ROI of cells in each tube was selected and the signal intensity was measured using ImageJ software.

2-3-7 *In vivo* MRI studies

N87 and SUIT2 tumors-bearing mice were prepared according to the method in Chapter 1. The scFv-IONPs or PEG-IONPs (60 mg iron/kg (33.2 nmol IONP/kg), 200 μL) were injected into the tumor-bearing mice *via* the tail vein. For *in vivo* blocking studies, the mixture of scFv-IONPs and

trastuzumab (24 mg/kg, n_{scFv}:$n_{trastuzumab}$ = 1:10) was intravenously injected into mice. MR images were taken with φ30 mm RF coil of MRmini SA before injection and 24 h after injection under the following condition: 2D-MS, *T2*W, Average = 4; TR = 4000 ms; TE = 70 ms; slice thickness = 2 mm; slice number = 17. The time point was decided based on our previous result that the highest accumulation of scFv-IONPs in N87 tumor along with the high tumor-to-blood ratio was observed 24 h after intravenous injection[34]. Water was used as a signal reference. ROI of each slice of tumors was drawn and the signal intensity was measured using ImageJ software. The ratio of tumor-to-phantom in each slice was calculated, and then post/pre-injection ratios were analyzed. The percentage of decrease in MR signal ($[1-({}_{post}ROI_{tumor}/{}_{post}ROI_{phantom})/({}_{pre}ROI_{tumor}/{}_{pre}ROI_{phantom})]\times100\%$) was calculated and shown in Figure 2-3.

2-3-8 IONPs staining

After *in vivo* MR studies, the mice injected with scFv-IONPs or PEG-IONPs were sacrificed, and the N87 and SUIT2 tumors were excised. The excised tumors were frozen, and cut into 10-μm-thick sections. Iron staining was performed using Berlin blue staining set (Wako Pure Chemical Industries, Ltd., Osaka, Japan). The tumor slices were then stained with Nuclear fast red (Sigma-Aldrich Co., St. Louis, MO, USA) and observed with microscope (BIOREVO BZ-9000, KEYENCE Co., Osaka, Japan).

2-3-9 Statistical analysis

Each experiment was performed at least thrice. For the *in vivo* experiment n = 5 mice were used. Statistical significance among groups was identified using the Dunnett method and Tukey-Kramer method for *in vitro* and *in vivo* experiments respectively. Data are presented as the mean ± standard deviation. *P* values of less than 0.05 were considered statistically significant.

Chapter 3

Preparation and investigation of the feasibility of using trastuzumab-conjugated liposomes encapsulated with IONPs as PA and MR dual-imaging probes (digest)

In Chapter 2, we described IONPs conjugated with anti-HER2 antibody derivatives (scFv-IONPs), which have been reported as potential probes for both PAI and MRI[34,35]. The probe showed HER2-specific tumor uptake, whereas > 10 times the amount of IONPs was needed to achieve PA tumor imaging than needed by MRI, which indicated the need to improve the imaging sensitivity of the probe, especially when used as a PAI agent.

Multiple studies have reported the marked enhancement of PA signals when the PA probes form aggregates[36,37]. A possible enhancement process is that when a nanomaterial with a high thermal conductivity absorbs light energy delivered by nanosecond laser pulses, heat occurs inside the nanomaterial, and it is quickly transferred to the surrounding medium. The thermal flux results in a thermal field around a single nanomaterial. In this case, the PA signal produced from a nanomaterial stems from the thermoelastic expansion that occurs when the surrounding medium is locally heated. The close proximity of an aggregate nanomaterial may result in overlapping thermal fields. This overlap would lead to amplification of the PA signal because overlapping thermal fields cause an increase in the rate of thermal flux and enhancement of the PA signal strength[38-40]. These facts indicate that the density of PA probes might be a key factor in determining the sensitivity of PA signals.

On the basis of previous papers and the hypothesis above, the author designed and synthesized PA probes having IONPs inside liposomes at a high concentration, and then conjugated anti-HER2 monoclonal antibody (trastuzumab) to the surface of liposomes (Tra-Lipo-IONPs) for targeting of HER2-positive tumors. Fluorescent lipids were included in liposomes for fluorescence tracking in

cellular uptake studies. A radioisotope labeling method was also constructed for *in vitro* binding study and biodistribution study.

PA and MR phantom studies were conducted by using Tra-Lipo-IONPs and dispersed IONPs, which resulted in the improvement of the signal intensity for both PAI and MRI. A cellular uptake study using fluorescence microscopy and iron staining demonstrated HER2-specific binding of Tra-Lipo-IONPs *in vitro* and the co-localization of lipids forming the liposomes and IONPs. A cellular binding study using ^{125}I-labeled Tra-Lipo-IONPs showed HER2-specific binding of Tra-Lipo-IONPs *in vitro*, which agreed with the results of an *in vitro* fluorescence microscopy study. *In vitro* PAI and MRI studies have also demonstrated HER2-specific binding of Tra-Lipo-IONPs. Among the series of probes, the one with highest binding affinity was selected for further evaluation. In the biodistribution study 1 h after probe injection, Tra-Lipo-IONPs accumulated specifically in HER2 positive tumors with higher tumor-to-blood ratios than those when using dispersed Tra-IONPs. These results suggested that Tra-Lipo-IONPs had potential as a sensitive PA/MR dual imaging probe targeting HER2.

Conclusion

In the present study, the author reaches a conclusion as follows.

1) In Chapter 1, based on gold nanorods (AuNRs), a series of trastuzumab-conjugated AuNRs with different amounts of ligand conjugation was synthesized and evaluated as potential PA/SPECT dual-imaging probes. Among the series, Tra2-AuNRs showed the best selective accumulation to HER2-positive N87 tumors in biodistribution studies as well as good affinity to N87 cells. Tra2-AuNRs also achieved N87-selective tumor imaging 96 h after probe injection in a SPECT study. These results suggested that Tra2-AuNRs may be a PA/SPECT dual imaging probe targeting HER2-positive tumors.
2) In Chapter 2, to achieve high-contrast *in vivo* imaging of HER2 at an earlier time point post-injection, iron oxide nanoparticles (IONPs) were used instead of AuNRs as the probe vehicle. Because IONPs are used as *T2*-weighted contrast agent in MRI, they were evaluated as a potential PA/MR dual-imaging probe. Anti-HER2 single chain Fv (scFv)-conjugated IONPs showed high binding affinity toward HER2 as well as HER2 selective PA/MR dual imaging both *in vitro* and *in vivo,* which indicated its potential usage as a robust cancer-targeted PA/MR dual imaging probe.
3) In Chapter 3, to achieve highly sensitive PA signals, we used trastuzumab-conjugated liposomes encapsulating IONPs at a high density (Tra-Lipo-IONPs). A series of liposomes with different amounts of ligand conjugation were designed, synthesized and evaluated. Significantly higher PA and MR signals for these liposomes than for dispersed IONPs were observed. Among the series, Tra300-Lipo-IONPs showed the highest binding affinity and HER2-specific PA/MR imaging *in vitro*. Tra300-Lipo-IONPs also specifically accumulated in HER2-positive tumors at 1 h post-injection with higher tumor-to-blood ratios than those achieved with dispersed Tra-IONPs. These results suggest that Tra300-Lipo-IONPs have a potential as a sensitive PA/MR dual imaging probe

targeting HER2.

In this thesis, the author developed pre-operative and intra-operative dual-imaging probes based on metal nanoparticles (AuNRs and IONPs) targeting HER2. Among all the probes discussed, Tra300-Lipo-IONPs showed the best potential as a pre-operative (MR) and intra-operative (PA) probe for HER2-targeted tumor imaging. These data provide useful information for the development of imaging probes applicable for pre- and intra-operative diagnoses and precise cancer therapy.

References

1. Bray, F., Ferlay, J., Soerjomataram, I., Siegel, R. L., Torre, L. A., Jemal, A. (2018). Global cancer statistics 2018: GLOBOCAN estimates of incidence and mortality worldwide for 36 cancers in 185 countries. CA: a Cancer Journal for Clinicians, 68(6), 394-424.
2. Nagao, M., Tsugane, S. (2016). Cancer in Japan: prevalence, prevention and the role of heterocyclic amines in human carcinogenesis. Genes and Environment, 38(1), 16-23.
3. Aliperti, L. A., Predina, J. D., Vachani, A., Singhal, S. (2011). Local and systemic recurrence is the Achilles heel of cancer surgery. Annals of Surgical Oncology, 18(3), 603-607.
4. Jiang, J. X., Keating, J. J., De Jesus, E. M., Judy, R. P., Madajewski, B., Venegas, O., Okusanya, O.T., Singhal, S. (2015). Optimization of the enhanced permeability and retention effect for near-infrared imaging of solid tumors with indocyanine green. American Journal of Nuclear Medicine and Molecular Imaging, 5(4), 390-400.
5. Tanaka, T., Terai, Y., Ono, Y. J., Fujiwara, S., Tanaka, Y., Sasaki, H., Tsunetoh, S., Kanemura, M., Yamamoto, K., Yamamoto, T., Ohmichi, M. (2015). Preoperative MRI and intraoperative frozen section diagnosis of myometrial invasion in patients with endometrial cancer. International Journal of Gynecological Cancer, 25(5), 879-883.
6. Arita, J., Ono, Y., Takahashi, M., Inoue, Y., Takahashi, Y., Matsueda, K., Saiura, A. (2015). Routine preoperative liver-specific magnetic resonance imaging does not exclude the necessity of contrast-enhanced intraoperative ultrasound in hepatic resection for colorectal liver metastasis. Annals of Surgery, 262(6), 1086-1091.
7. Xiao, Q., Chen, T., Chen, S. (2018). Fluorescent contrast agents for tumor surgery. Experimental and Therapeutic Medicine, 16(3), 1577-1585.
8. Nie, J., Zhang, J., Gao, J., Guo, L., Zhou, H., Hu, Y., Zhu, C., Li, Q., Ma, X. (2017). Diagnostic role of ^{18}F-FDG PET/MRI in patients with gynecological malignancies of the pelvis: A systematic review and meta-analysis. PloS One, 12(5), e0175401.
9. Zhu, D., Wang, L., Zhang, H., Chen, J., Wang, Y., Byanju, S., Liao, M. (2017). Prognostic value of ^{18}F-FDG-PET/CT parameters in patients with pancreatic carcinoma: A systematic review and meta-analysis. Medicine, 96(33), e7813.
10. Nomori, H., Cong, Y., Sugimura, H. (2016). Utility and pitfalls of sentinel node identification using indocyanine green during segmentectomy for cT1N0M0 non-small cell lung cancer. Surgery Today, 46(8), 908-913.
11. Kim, H. K., Quan, Y. H., Choi, B. H., Park, J. H., Han, K. N., Choi, Y., Kim, B. M., Choi, Y. H. (2015). Intraoperative pulmonary neoplasm identification using near-infrared fluorescence imaging. European Journal of Cardio-Thoracic Surgery, 49(5), 1497-1502.

12. Tam, A. C. (1986). Applications of photoacoustic sensing techniques. Reviews of Modern Physics, 58(2), 381-431.
13. Kanazaki, K., Sano, K., Makino, A., Yamauchi, F., Takahashi, A., Homma, T., Ono, M., Saji, H. (2016). Feasibility of poly (ethylene glycol) derivatives as diagnostic drug carriers for tumor imaging. Journal of Controlled Release, 226, 115-123.
14. Jain, P. K., Lee, K. S., El-Sayed, I. H., El-Sayed, M. A. (2006). Calculated absorption and scattering properties of gold nanoparticles of different size, shape, and composition: applications in biological imaging and biomedicine. The Journal of Physical Chemistry B, 110(14), 7238-7248.
15. Matsumura, Y., Maeda, H. (1986). A new concept for macromolecular therapeutics in cancer chemotherapy: mechanism of tumoritropic accumulation of proteins and the antitumor agent smancs. Cancer Research, 46(12 Part 1), 6387-6392.
16. Pouliquen, D., Le Jeune, J. J., Perdrisot, R., Ermias, A., Jallet, P. (1991). Iron oxide nanoparticles for use as an MRI contrast agent: pharmacokinetics and metabolism. Magnetic Resonance Imaging, 9(3), 275-283.
17. Slamon, D. J., Godolphin, W., Jones, L. A., Holt, J. A., Wong, S. G., Keith, D. E., Levin, W. J., Stuart, S. G., Udove, J., Ullrich, A. (1989). Studies of the HER-2/neu proto-oncogene in human breast and ovarian cancer. Science, 244(4905), 707-712.
18. Hori, M., Matsuda, T., Shibata, A., Katanoda, K., Sobue, T., Nishimoto, H., Japan Cancer Surveillance Research Group (2015). Cancer incidence and incidence rates in Japan in 2009: a study of 32 population-based cancer registries for the Monitoring of Cancer Incidence in Japan (MCIJ) project. Japanese Journal of Clinical Oncology, 45(9):884-891.
19. Luo, G. F., Chen, W. H., Lei, Q., Qiu, W. X., Liu, Y. X., Cheng, Y. J., Zhang, X. Z. (2016). A triple-collaborative strategy for high-performance tumor therapy by multifunctional mesoporous silica-coated gold nanorods. Advanced Functional Materials, 26(24), 4339-4350.
20. Zhang, P., Wang, Y., Lian, J., Shen, Q., Wang, C., Ma, B., Zhang, Y., Xu, T., Li, J., Shao, Y., Xu, F., Zhu, J. J. (2017). Engineering the surface of smart nanocarriers using a pH-/thermal-/GSH-responsive polymer zipper for precise tumor targeting therapy *in vivo*. Advanced Materials, 29(36), 1702311-1702320.
21. Zhao, X., Yang, C. X., Chen, L. G., Yan, X. P. (2017). Dual-stimuli responsive and reversibly activatable theranostic nanoprobe for precision tumor-targeting and fluorescence-guided photothermal therapy. Nature Communications, 8, 14998-15006.
22. Chauhan, V. P., Jain, R. K. (2013). Strategies for advancing cancer nanomedicine. Nature Materials, 12(11), 958-962.
23. An, L., Wang, Y., Tian, Q., Yang, S. (2017). Small gold nanorods: Recent advances in synthesis, biological imaging, and cancer therapy. Materials, 10(12), 1372.
24. Martínez, J. C., Chequer, N. A., González, J. L., Cordova, T. (2012). Alternative metodology for

gold nanoparticles diameter characterization using PCA technique and UV-Vis spectrophotometry. Nanoscience and Nanotechnology, 2(6), 184-189.

25. Wagner, V., Dullaart, A., Bock, A. K., Zweck, A. (2006). The emerging nanomedicine landscape. Nature Biotechnology, 24(10), 1211-1217.
26. Wang, Y. X. J., Hussain, S. M., Krestin, G. P. (2001). Superparamagnetic iron oxide contrast agents: physicochemical characteristics and applications in MR imaging. European Radiology, 11(11), 2319-2331.
27. J Wang, Y. X., Xuan, S., Port, M., Idee, J. M. (2013). Recent advances in superparamagnetic iron oxide nanoparticles for cellular imaging and targeted therapy research. Current Pharmaceutical Design, 19(37), 6575-6593.
28. Ittrich, H., Peldschus, K., Raabe, N., Kaul, M., Adam, G. (2013). Superparamagnetic iron oxide nanoparticles in biomedicine: applications and developments in diagnostics and therapy. RöFo-Fortschritte auf dem Gebiet der Röntgenstrahlen und der bildgebenden Verfahren, 185(12), 1149-1166.
29. Wahajuddin, S. A. (2012). Superparamagnetic iron oxide nanoparticles: magnetic nanoplatforms as drug carriers. International Journal of Nanomedicine, 7, 3445-3471.
30. Rudin, M., Rausch, M., Stoeckli, M. (2005). Molecular imaging in drug discovery and development: potential and limitations of nonnuclear methods. Molecular Imaging and Biology, 7(1), 5-13.
31. Armanetti, P., Flori, A., Avigo, C., Conti, L., Valtancoli, B., Petroni, D., Doumettd, S., Cappiellod, L., Cappiellod, C., Baldid, G., Bencinic, A., Menichetti, L. (2018). Spectroscopic and photoacoustic characterization of encapsulated iron oxide super-paramagnetic nanoparticles as a new multiplatform contrast agent. Spectrochimica Acta Part A: Molecular and Biomolecular Spectroscopy, 199, 248-253.
32. Moore, A., Weissleder, R., Bogdanov Jr, A. (1997). Uptake of dextran‐coated monocrystalline iron oxides in tumor cells and macrophages. Journal of Magnetic Resonance Imaging, 7(6), 1140-1145.
33. Keliher, E. J., Yoo, J., Nahrendorf, M., Lewis, J. S., Marinelli, B., Newton, A., Pittet, M. J., Weissleder, R. (2011). ^{89}Zr-labeled dextran nanoparticles allow *in vivo* macrophage imaging. Bioconjugate Chemistry, 22(12), 2383-2389.
34. Kanazaki, K., Sano, K., Makino, A., Shimizu, Y., Yamauchi, F., Ogawa, S., Ding, N., Yano, T., Temma, T., Ono, M.,Saji, H. (2015). Development of anti-HER2 fragment antibody conjugated to iron oxide nanoparticles for *in vivo* HER2-targeted photoacoustic tumor imaging. Nanomedicine: Nanotechnology, Biology and Medicine, 11(8), 2051-2060.
35. Ding, N., Sano, K., Kanazaki, K., Ohashi, M., Deguchi, J., Kanada, Y., Ono, M., Saji, H. (2016). *In vivo* HER2-targeted magnetic resonance tumor imaging using iron oxide nanoparticles

conjugated with anti-HER2 fragment antibody. Molecular Imaging and Biology, 18(6), 870-876.

36. Ju, K. Y., Kang, J., Pyo, J., Lim, J., Chang, J. H., Lee, J. K. (2016). pH-Induced aggregated melanin nanoparticles for photoacoustic signal amplification. Nanoscale, 8(30), 14448-14456.
37. Bayer, C. L., Nam, S. Y., Chen, Y. S., Emelianov, S. Y. (2013). Photoacoustic signal amplification through plasmonic nanoparticle aggregation. Journal of Biomedical Optics, 18(1), 016001.
38. Smith, B. R., Gambhir, S. S. (2017). Nanomaterials for *in vivo* imaging. Chemical Reviews, 117(3), 901-986.
39. Willets, K. A., Stranahan, S. M., Weber, M. L. (2012). Shedding light on surface-enhanced Raman scattering hot spots through single-molecule super-resolution imaging. The Journal of Physical Chemistry Letters, 3(10), 1286-1294.
40. Cheng, K., Kothapalli, S. R., Liu, H., Koh, A. L., Jokerst, J. V., Jiang, H., Yang, M., Li, J., Levi, J., Wu, J. C., Gambhir, S. S., Cheng, Z. (2014). Construction and validation of nano gold tripods for molecular imaging of living subjects. Journal of the American Chemical Society, 136(9), 3560-3571.

Acknowledgements

I am extremely lucky to have had the chance to work with Professor Hideo Saji, Professor Masahiro Ono and Dr. Kohei Sano on the ideas in this dissertation, and I would very much like to thank them for their support. Professor Saji took me on as a graduate student, opened the door towards the patho-functional bioanalysis field, and encouraged me to pursue the goal that I had a passion for. Dr. Sano is the one that originally drew me to the development of cancer imaging. Dr. Sano instructed me from the very base of research and inspired me hugely with his contagious enthusiasm and outlook on research. I could not have asked for a better mentor and I feel very grateful from the bottom of my heart for his generosity with his time, experience and thoughts. I would also like to thank Professor Ono, who gave me constructive ideas and suggestions constantly through the years both academically and in life, and who was always generous with his time.

I am grateful to Dr. Yoichi Shimizu and Dr. Hiroyuki Watanabe for consistently sharing practical and thoughtful advices. Thanks also to Dr. Hiroyuki Kimura for all the help he offered concerning the operation of MRI related devices.

I would also like to thank Dr. Kengo Kanazaki for having taught me many experimental techniques and have given me many experimental suggestions, as well as Professor Takeshi Namita, Graduate School of Medicine, for all the help and support provided on PA experiments.

I would like to thank all my wonderful friends and colleagues at the Patho-functional bioanalysis lab. I would especially like to thank Manami Ohashi, Yuko Kanada and Jun Deguchi for all those helpful discussions and suggestions, and for having helped make my days in the lab enjoyable. I would also like to thank Ms. Aya Ono for helping me start daily life in Japan smoothly, and Ms. Saeko Terai for all the help on RI related routines. Thanks also to other colleagues in the lab, including Dr. Shinpei Iikuni, Haruka Okuda, Yuki Doi, Sho Kaide, Masaru Fujinohara, Naoki Mastushita, Yuya Okada,

Kiyoshiro Kawano, Kouji Mastuyoshi, Yusuke Miki, Keiichi Tanimura, Kengo Fukui, Futa Itagaki, Shiori Sakai, Haruka Tastumi, Yukihiro Nakai, Masato Ando, Yuki Idoko, Ichiro Kamei, Mari Suzukita, Yuuta Tarumizu.

Thank you to Victor Hugo, Alan Rickman, J.K.Rowling and Lin-Manuel Miranda for your absolute talent and humanity, and for inspiring me to create a vision for life. To Mat Baynton and Jonny Phillips for the laughter and happy memories. To my dearest friends Chunjiao Zhou, Ting Xiao, Hongxue Ni and Xueming Xia for your time, love, thoughts and company. You kept me alive.

Finally, I would like to thank my parents for their love and support. I simply cannot think of anyone more supportive for providing me with guidance and encouragement and allowing me to be what I was always meant to be.